Few-Body Systems 24, 55–79 (1998)

Few-Body Systems

Two-Body *T*-Matrices Without Angular-Momentum Decomposition: Energy and Momentum Dependences

Ch. Elster[1], J. H. Thomas[1], and W. Glöckle[2]

[1] Institute of Nuclear and Particle Physics and Department of Physics, Ohio University, Athens, OH 45701, USA

[2] Institute for Theoretical Physics II, Ruhr-University Bochum, D-44780 Bochum, Germany

Abstract. The two-body *T*-matrix is calculated directly as function of two vector momenta for different Malfliet-Tjon-type potentials. At a few hundred MeV projectile energy the total amplitude is quite a smooth function showing only a strong peak in forward direction. In contrast, the corresponding partial-wave contributions, whose number increases with increasing energy, become more and more oscillatory with increasing energy. The angular and momentum dependence of the full amplitude is studied and displayed on as well as off the energy shell as function of positive and negative energies. The behaviour of the *T*-matrix in the vicinity of bound-state poles and resonance poles in the second energy sheet is studied. It is found that the angular dependence of *T* exhibits very characteristic properties in the vicinity of those poles, which are given by the Legendre function corresponding to the quantum number either of the bound state or the resonance (or virtual) state. This behaviour is illustrated along numerical examples.

1 Introduction

At low energies in the MeV and the few tenth of MeV region very few angular momenta contribute to the nucleon-nucleon (*NN*) scattering process. Consequently a description using angular-momentum decomposition is an adequate tool for carrying out scattering calculations. However, at intermediate energies, i.e., energies of a few hundred MeV, and higher energies very many angular momenta contribute to the scattering amplitude. In these energy domains those individual contributions to the scattering amplitude for a fixed high angular momentum oscillate strongly in angle, whereas the total amplitude is much smoother. This suggests the direct determination of *T* as function of the initial- and final-momentum vectors avoiding angular-momentum decomposition totally. For *NN* scattering, investigations of this kind have already been undertaken [1–4].

The choice of momentum vectors as adequate variables is also suggested from the *NN* force. The dependence on momentum vectors in the case of the widely used

one-boson-exchange forces is, for instance, rather simple, whereas the partial-wave representation of this force leads to complicated expressions [5]. This is already apparent in the most simple case of a scalar meson propagator, $1/((\mathbf{q}' - \mathbf{q})^2 + \mu^2)$, which is the central ingredient to any *NN* force. In a partial-wave decomposition this is represented in the form $(1/q'q)Q_l(z)$, where $z = (\mathbf{q}'^2 + \mathbf{q}^2 + \mu^2)/2q'q$ and $Q_l(z)$ is the Legendre function of the second kind. For large values of l the latter requires some care in order to be handled correctly in numerical calculations.

Scattering of more than two particles requires two-body T-matrices off-the-energy-shell (off-shell for short notation) as dynamical input, which are apparently easier to handle if they enter the calculations as smooth functions instead of strongly varying partial-wave components. Of course, these remarks also apply to the treatment of scattering processes of more than two particles at intermediate energies, which themselves are also treated more economically and transparently using momentum vectors instead of partial-wave representations. Calculations of three and more particles use as input fully off-shell two-body T-matrices, whose properties as functions of arbitrary initial and final momenta and in general positive and negative energies should be well understood. Specifically at negative energies there may be bound-state poles and in the second energy sheet there may be poles related to virtual states and resonances.

Our aim in this article is to generate two-body T-matrices directly in a three-dimensional form and display their properties as functions of the magnitudes of the off-shell momenta, the angle between the two momentum vectors and of the energy. We are not aware of a similar study of this generality in the literature. Usually, only partial-wave-projected amplitudes are displayed and discussed [6].

In Sect. 2 we describe our solution of the two-body Lippmann-Schwinger equation directly as function of the momentum vectors and illustrate the on- and off-shell properties of the resulting T-matrices obtained with simple Yukawa-type two-nucleon potentials. In Sect. 3 we discuss the pole structure of the T-matrix as function of the energy and illustrate its angular and energy behaviour at and around bound-state poles. In Sect. 4 we illustrate the behaviour of the T-matrix for virtual and resonant states in the second energy sheet. We conclude in Sect. 5.

2 The On- and Off-Shell Two-Body T-Matrix at Positive Energies

Two-body scattering is governed by the Lippmann-Schwinger equation

$$T = V + VG_0T, \tag{2.1}$$

where V is the two-body (e.g., two-nucleon) potential, $G_0 = (z - H_0)^{-1}$ the free two-body propagator, and T the transition operator. In momentum space its matrix elements $T(\mathbf{q}', \mathbf{q}, z) \equiv \langle \mathbf{q}'|T(z)|\mathbf{q}\rangle$ obey the integral equation

$$T(\mathbf{q}', \mathbf{q}, z) = V(\mathbf{q}', \mathbf{q}) + \int d^3q''\ V(\mathbf{q}', \mathbf{q}'') \frac{1}{z - \dfrac{q''^2}{m}} T(\mathbf{q}'', \mathbf{q}, z). \tag{2.2}$$

Here, $\mathbf{q}$ are the relative momenta, m the mass of each of the two particles and z an arbitrary energy. In the case of particles with unequal masses, the quantity m in Eq. (2.2) is to be replaced by two times the reduced mass of the system. We use a nonrelativistic

framework. In this article we restrict ourselves to two spinless particles and local potentials. Therefore, $V(\mathbf{q}', \mathbf{q})$ as well as $T(\mathbf{q}', \mathbf{q}, z)$ are scalar functions

$$V(\mathbf{q}', \mathbf{q}) = V(q', q, \hat{\mathbf{q}}' \cdot \hat{\mathbf{q}}) \tag{2.3}$$

and

$$T(\mathbf{q}', \mathbf{q}) = T(q', q, \hat{\mathbf{q}}' \cdot \hat{\mathbf{q}}). \tag{2.4}$$

In Eq. (2.4) we dropped the parametric dependence on the energy z. This notation then leads to the following explicit form of Eq. (2.2)

$$T(q', q, x') = V(q', q, x') + \int_0^\infty dq''\ q''^2 \int_{-1}^{1} dx'' \int_0^{2\pi} d\varphi''\ V(q', q'', y) \frac{1}{z - \dfrac{q''^2}{m}} T(q'', q, x''), \tag{2.5}$$

where $x' = \hat{\mathbf{q}}' \cdot \hat{\mathbf{q}}$, $x'' = \hat{\mathbf{q}}'' \cdot \hat{\mathbf{q}}$, and $y = \hat{\mathbf{q}}'' \cdot \hat{\mathbf{q}}'$. We can express y through x' and x'' as

$$y = x'x'' + \sqrt{1 - x'^2}\sqrt{1 - x''^2} \cos\varphi'', \tag{2.6}$$

where the arbitrary azimuthal angle φ for $\hat{\mathbf{q}}$ is chosen to be zero. If we define

$$v(q', q, x', x) \equiv \int_0^\infty d\varphi\ V(q', q, x'x + \sqrt{1 - x'^2}\sqrt{1 - x^2} \cos\varphi), \tag{2.7}$$

the integral equation (2.5) becomes

$$T(q', q, x') = \frac{1}{2\pi} v(q', q, x', 1) + \int_0^\infty dq''\ q''^2 \int_{-1}^{1} dx''\ v(q', q'', x', x'') \frac{1}{z - \dfrac{q''^2}{m}} T(q'', q, x''). \tag{2.8}$$

This is a two-dimensional integral equation in the off-shell momenta q' (q'') and the cosine of the 'scattering angle' x' (x'').

In this section we consider the solutions of the integral equation (2.8) at positive energies, i.e., we choose $z \equiv E + i\varepsilon = (q_0^2/m) + i\varepsilon$, corresponding to the incoming momentum $\mathbf{q}_0$. In order to obtain insight into the behaviour of the T-matrix, we shall consider the on-shell element $T(q_0, q_0, x, E)$, whose square is proportional to the differential cross section, as well as the half-off-shell, $T(q, q_0, x, E)$, and fully off-shell, $T(q, q', x, E)$, T-matrix.

We solve the two-dimensional integral equation typically using 24 or 32 q-points and 24 x-points. The Cauchy singularity is separated into a principal-value part and a δ-function part, and the principal-value singularity is treated by subtraction. The integration interval for the q-integration is covered by mapping the Gauss-Legendre points u from the interval (0, 1) via

$$q = b \tan\left(\frac{\pi}{2} u\right)$$

to the interval (0, ∞). Typical values of b are 1000 MeV/c.

A very stringent test for our numerics is the off-shell unitarity relation, which is a direct consequence of Eq. (2.2). In our two-dimensional form it reads

$$\text{Im } T(q', q, x') = -\frac{\pi}{2} m q_0 \int_{-1}^{1} dx'' \int_0^{2\pi} d\varphi''\ T(q', q_0, y) T^*(q, q_0, x''), \tag{2.9}$$

where y is given in Eq. (2.6). With Eq. (2.9) we allowed for the most general case of the unitarity relation, where the energy $z = E = q_0^2/m$ is not related to the incoming momentum q, thus $q \neq q' \neq q_0$. In our numerical tests Eq. (2.9) was fulfilled for arbitrary q', q, and x' values to an accuracy better than 0.001% with the above quoted number of integration points.

As main application we choose potentials of the Malfliet-Tjon [7] type, i.e.

$$V(r) = V_r \frac{\exp[-\mu_R r]}{r} - V_A \frac{\exp[-\mu_A r]}{r}, \tag{2.10}$$

and consequently

$$V(\mathbf{q}', \mathbf{q}) = \frac{1}{2\pi^2} \left(\frac{V_R}{(\mathbf{q}' - \mathbf{q})^2 + \mu_R^2} - \frac{V_A}{(\mathbf{q}' - \mathbf{q})^2 + \mu_A^2} \right). \tag{2.11}$$

In the case of a Malfliet-Tjon-type potential the φ-integration of Eq. (2.7) can be carried out analytically with the result

$$v(q', q, x', x) = \frac{1}{\pi} \left[\frac{V_R}{\sqrt{(q'^2 + q^2 - 2q'qx'x + \mu_R^2)^2 - 4q'^2 q^2 (1 - x'^2)(1 - x^2)}} \right.$$
$$\left. - \frac{V_A}{\sqrt{(q'^2 + q^2 - 2q'qx'x + \mu_A^2)^2 - 4q'^2 q^2 (1 - x'^2)(1 - x^2)}} \right]. \tag{2.12}$$

The parameters used for V are given as $V^{(\mathrm{I})}$ in Table 1. Note that they are slightly different from the ones used in ref. [7].

As first numerical example we would like to demonstrate the connection of the angle-depended on-shell amplitude $T(q_0, q_0, x, E)$ and its representation in terms of partial-wave amplitudes,

$$T(q_0, q_0, x) = \sum_{l=0}^{\infty} \frac{2l+1}{4\pi} T_l(q_0) P_l(x), \tag{2.13}$$

where

Table 1. Parameters of the Malfliet-Tjon-type potentials. As conversion factor we use units such that $\hbar c = 197.3286\,\text{MeV fm} = 1$

	V_A	μ_A [MeV]	V_R	μ_R [MeV]
$V^{(\mathrm{I})}$	3.1769	305.86	7.291	613.69
$V^{(\mathrm{II})}$	6.0	305.86	7.291	613.69
$V^{(\mathrm{III})}$	5.1	305.86	7.291	613.69
$V^{(\mathrm{IV})}$	2.6047	305.86	7.291	613.69

$$T_l(q_0) = \frac{2}{\pi}\frac{1}{q_0 m}\exp[i\delta_l(q_0)]\sin\delta_l(q_0).$$

The quantity $\delta_l(q_0)$ is the phase shift for a given angular momentum l and is determined in the standard manner. In Fig. 1 we show Re $T(q_0, q_0, x, E)$ at 300 and 800 MeV

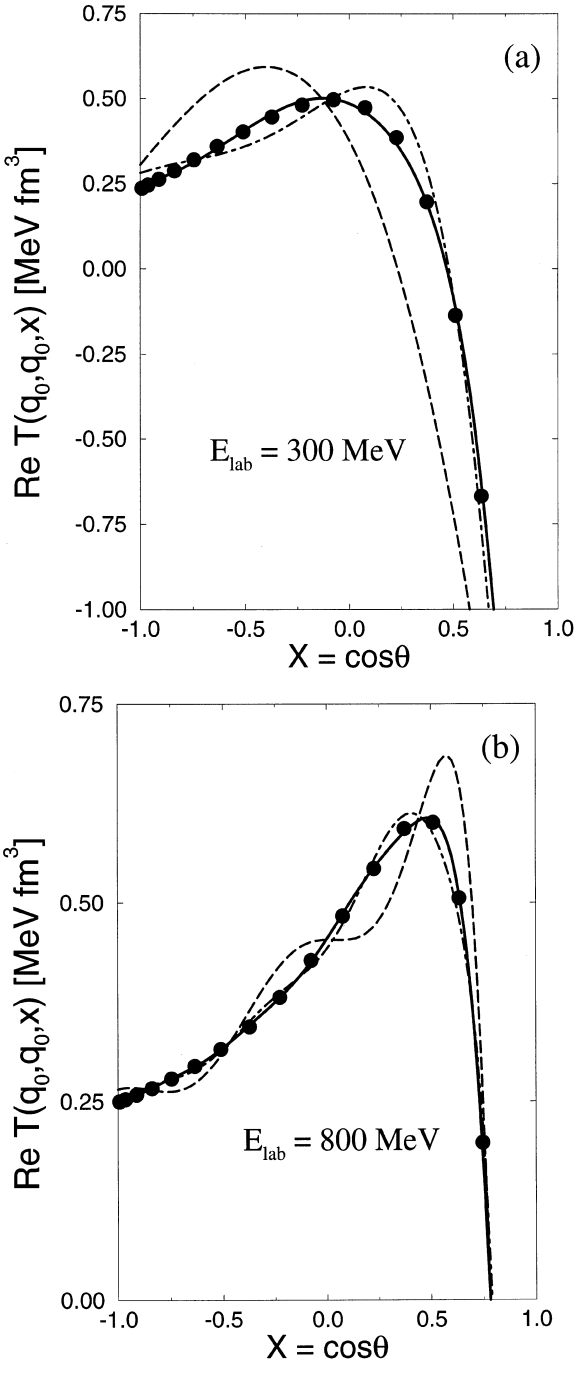

Fig. 1. Angular dependence of the real part of the on-shell *T*-matrix, Re $T(q_0, q_0, x, E)$. At $E_{\rm lab} = 300$ MeV, (**a**), the dashed line represents the partial-wave sum up to $j = 2$, the dashed-dotted line the sum up to $j = 4$, and the solid line the sum up to $j = 6$. The solid bullets stand for the calculation performed without angular-momentum decomposition. At $E_{\rm lab} = 800$ MeV, (**b**), the dashed line represents the partial-wave sum up to $j = 6$, the dashed-dotted line stands for the sum up to $j = 9$, and the solid line for the sum up to $j = 12$. Again, the solid bullets represent the calculation performed without angular-momentum decomposition

laboratory energies together with partial-wave sums up to a given angular momentum l. Note that $E = E_{\rm lab}/2$. The strong peak of Re $T(q_0, q_0, x, E)$ in forward direction requires high orders of Legendre polynomials for a correct description. This is, of course,

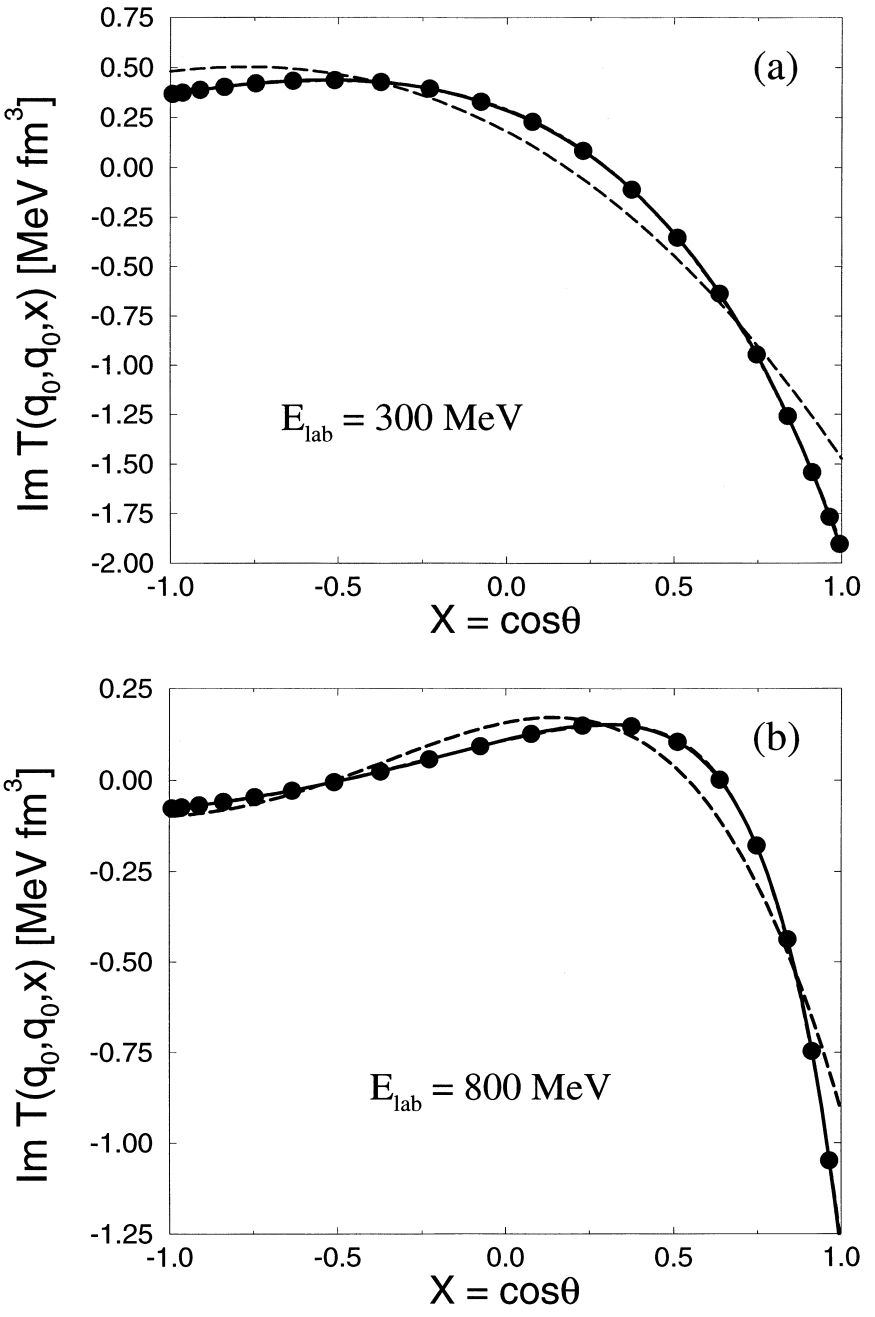

Fig. 2. Angular dependence of the imaginary part of the on-shell T-matrix, Im $T(q_0, q_0, x, E)$. At $E_{\rm lab} =$ 300 MeV, (**a**), the dashed line represents the partial-wave sum up to $j = 2$, the solid line the sum up to $j = 4$. The solid bullets stand for the calculation performed without angular-momentum decomposition. At $E_{\rm lab} =$ 800 MeV, (**b**), the dashed line represents the partial-wave sum up to $j = 3$, the solid line the sum up to $j = 6$. The bullets stand for the calculation performed without angular momentum decomposition

especially pronounced for the higher energy. In Fig. 2 we display Im $T(q_0, q_0, x, E)$ at the same energies together with its representation in partial-wave sums. It can be seen that Im $T(q_0, q_0, x, E)$ needs less partial-wave amplitudes for its correct representation, the reason being that Im T_l is proportional to $\sin^2 \delta_l$, whereas Re T_l is proportional to $\cos \delta_l \sin \delta_l$. For large values of l the phase shifts become small, thus Im T_l decreases with δ_l^2, whereas Re T_l only decreases proportional to δ_l.

An overview of the angular dependence of the full on-shell amplitude $T(q_0, q_0, x, E)$ as function of the energy is given in Fig. 3. Starting from a relatively flat angular distribution at lower energies the peaking in forward direction develops with increasing energy. At the same time the angular range, where the cross section is flat and small, becomes larger with increasing energy, indicating that forward scattering dominates at higher energies.

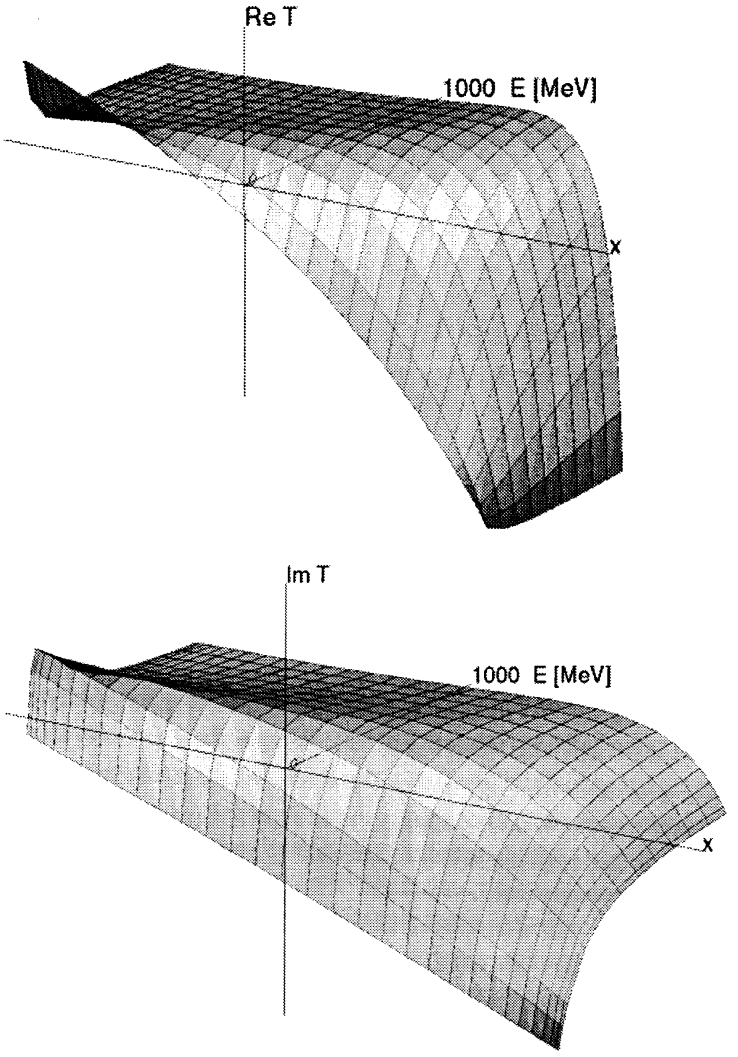

Fig. 3. Angular dependence of the real (up) and imaginary (down) parts of the on-shell *T*-matrix as function of the laboratory energy from $E_{\text{lab}} = 50$ MeV to $E_{\text{lab}} = 1000$ MeV

Next we consider the half-off-shell amplitude $T(q, q_0, x, E)$ for two energies. Fig. 4 shows that $T(q, q_0, x, E)$ is rather small and structureless for all off-shell momenta q, with the exception of q being close to the on-shell momentum q_0.

The most general amplitude, the fully off-shell amplitude $T(q, q', x, E)$ is displayed in Figs. 5 and 6 for its real part as function of the off-shell momentum q and the angle x for two fixed off-shell momenta q'. Contrary to what one might expect, the strongest forward peaking does not occur for q being close to the on-shell value, but for $q = q'$. This agrees with the behaviour of the driving term, which peaks for $q = q'$. We found this behaviour for all energies $E > 0$.

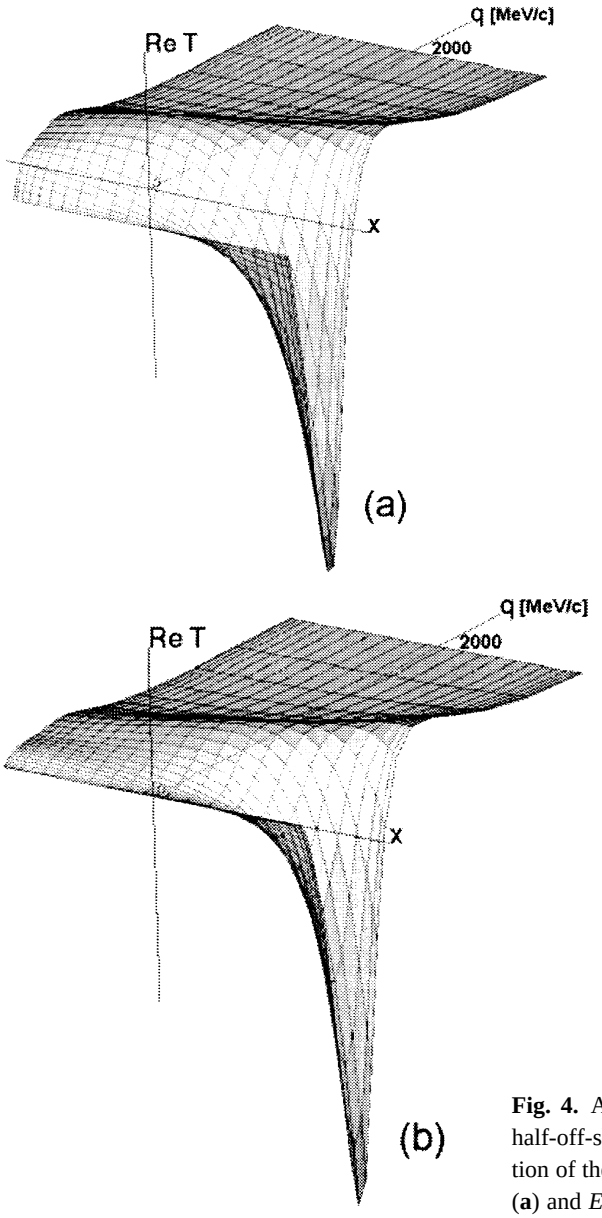

Fig. 4. Angular dependence of the real part of the half-off-shell T-matrices, Re $T(q, q_0, x, E)$, as function of the off-shell momentum q at $E_{\rm lab} = 200$ MeV (**a**) and $E_{\rm lab} = 500$ MeV (**b**)

All numerical and graphical examples considered so far refer to a potential of Malfliet-Tjon-type with repulsive and attractive parts (potential $V^{(I)}$ in Table 1). Its

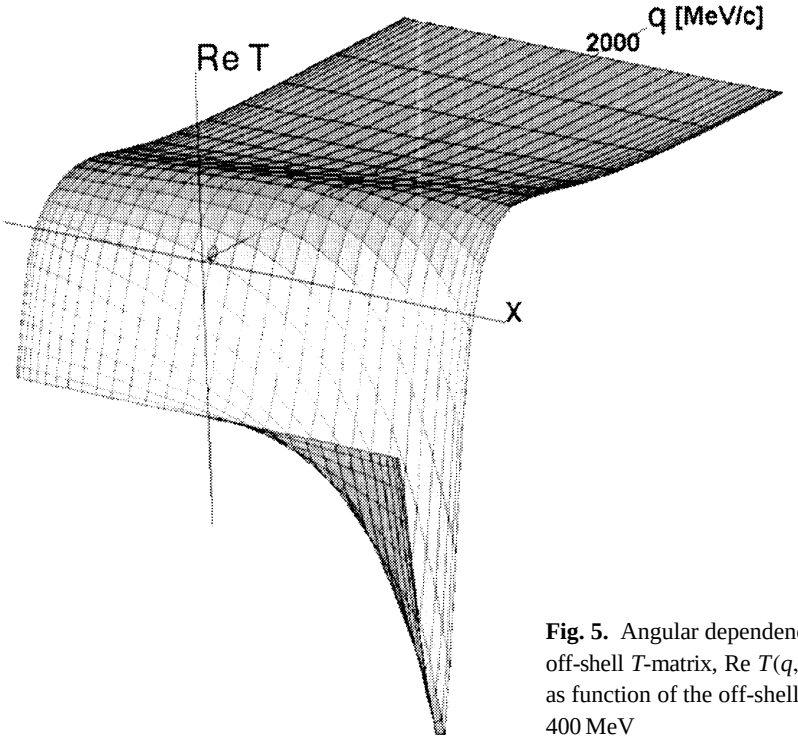

Fig. 5. Angular dependence of the real part of the off-shell *T*-matrix, Re $T(q, q' = 250\ \text{MeV}/c, x, E)$, as function of the off-shell momentum q at $E_{\text{lab}} = 400\,\text{MeV}$

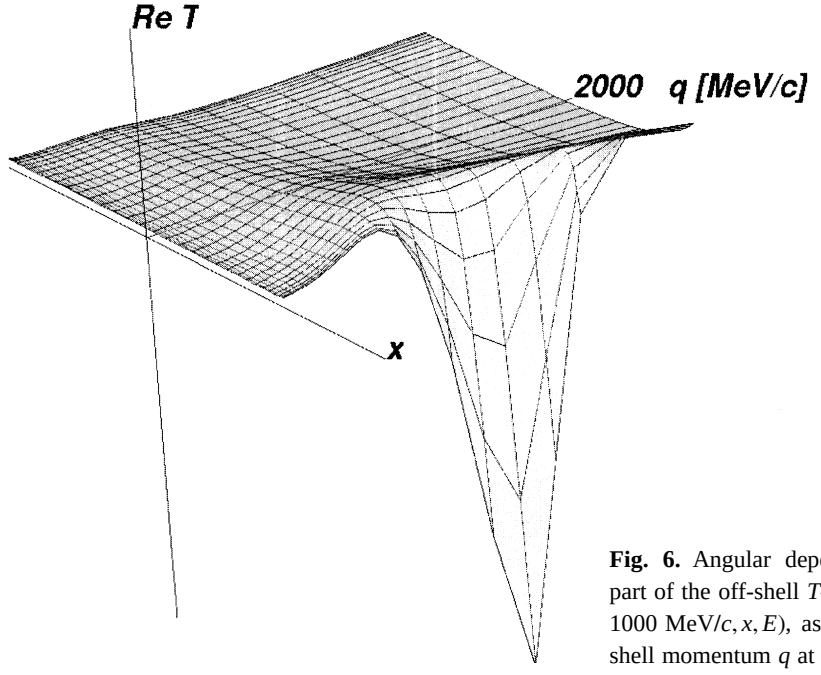

Fig. 6. Angular dependence of the real part of the off-shell *T*-matrix, $\text{Re}\,T(q, q' = 1000\ \text{MeV}/c, x, E)$, as function of the off-shell momentum q at $E_{\text{lab}} = 400\,\text{MeV}$

strength is such that it supports a bound state at $E = -2.23\,\mathrm{MeV}$. Though this potential is of quite simple character, it captures essential features of *NN* interaction models based on meson exchange with respect to the propagator structure.

3 The Off-Shell *T*-Matrix at Negative Energies

In the context of Faddeev-Yakubovsky equations two-body *T*-matrices need to be evaluated at negative energies. In a three-body system the energy argument for the two-body *T*-matrix is given as $E = E_{\mathrm{tot}} - (3/4m)q^2$ [9]. Here E_{tot} is the total energy of the three-particle system and $(3/4m)q^2$ is the kinetic energy of the relative motion of the third particle with respect to the interacting pair, which is described by the *T*-matrix. For an interacting three-body system the relative momentum $|\mathbf{q}|$ is not conserved. Therefore it can have arbitrary values and E covers all energies below E_{tot}. Thus we are interested to see, whether the angular dependence of the *T*-matrix evaluated at negative energies is similar to the one observed at positive energies. A second consideration is that bound states of the two-body system lead to poles in the *T*-matrix. The angular dependence at and around a pole should be dictated by the one of the bound state. We now investigate these questions and provide numerical illustrations.

The formal solution to the Lippmann-Schwinger equation, Eq. (2.1), is given by

$$T(z) = V + V\frac{1}{z-H}V, \tag{3.1}$$

where H is the full two-body Hamiltonian. If this Hamiltonian supports a bound state $|\phi_b\rangle$ at $z = E_b$, it follows immediately that

$$T(z) \xrightarrow{z\to E_b} V|\phi_b\rangle\frac{1}{z-E_b}\langle\phi_b|V. \tag{3.2}$$

In momentum-space representation, Eq. (3.2) reads

$$T(\mathbf{q}',\mathbf{q},z) \xrightarrow{z\to E_b} \langle\mathbf{q}'|V|\phi_b\rangle\frac{1}{z-E_b}\langle\phi_b|V|\mathbf{q}\rangle. \tag{3.3}$$

The bound state obeys $H|\phi_b\rangle = E_b|\phi_b\rangle$ and has a certain fixed angular momentum l, such that

$$\langle\mathbf{q}|\phi_b\rangle = \phi_{b,l}(q)Y_{lm}(\hat{\mathbf{q}}). \tag{3.4}$$

Since T is a scalar quantity, its behaviour at and around the pole has to have the form

$$\begin{aligned} T(\mathbf{q}',\mathbf{q},z) &\xrightarrow{z\to E_b} \sum_m Y_{lm}(\hat{\mathbf{q}}')g_l(q')\frac{1}{z-E_b}Y^*_{lm}(\hat{\mathbf{q}})g_l(q) \\ &= \frac{2l+1}{4\pi}P_l(\hat{\mathbf{q}}'\cdot\hat{\mathbf{q}})\frac{g_l(q')g_l(q)}{z-E_b} \\ &\equiv \frac{R_l(q',q,\hat{\mathbf{q}}'\cdot\hat{\mathbf{q}})}{z-E_b}. \end{aligned} \tag{3.5}$$

Here

$$g_l(q) = \int_0^\infty dq'\; q'^2 v_l(q,q')\phi_{b,l}(q') \tag{3.6}$$

with

$$v_l(q,q') = \frac{2}{\pi} \int_0^\infty dr\, r^2 j_l(qr) V(r) j_l(q'r). \tag{3.7}$$

From Eq. (3.6) it can clearly be seen that the angular dependence of T exhibits a very characteristic behaviour in the vicinity of the bound-state poles, which is given by the Legendre function corresponding to the angular quantum number of the bound state. In order to illustrate the pole behaviour, we choose the potential $V^{(\mathrm{II})}$ of Table 1, which supports a s-wave bound state at $E_s = -190.16$ MeV and a p-wave bound state at $E_p = -14.629$ MeV. These binding energies are determined in a standard manner solving the Schrödinger equation for a fixed angular momentum. This is a simple, one-dimensional problem, whose solution also provides the function $g_l(q)$ and thus the residue $R_l(q', q, \hat{\mathbf{q}}' \cdot \hat{\mathbf{q}})$ from Eq. (3.6). The values of the binding energies can also be obtained by solving the two-dimensional integral equation (2.8) and determining the pole position from the solution. Choosing the same integration points q in the partial-wave-projected, one-dimensional form and the two-dimensional form, the bound-state energies E_b agree very well with the pole positions E_{pol}. For example, for 40 q-points (and 32 x-points) we find $E_b(l=0) = -190.162$ MeV, which has to be compared to $E_{\mathrm{pol}}(l=0) = -190.164$ MeV. Similarly, we find $E_b(l=1) = -14.6296$ MeV compared to $E_{\mathrm{pol}}(l=1) = -14.6296$ MeV. These results can be pushed to higher accuracy if desired. We also determine the residues at each pole from the solution of the two-dimensional integral equation and illustrate our result in Table 2 for the arbitrary choice of $q' = q = q_0 = \sqrt{m|E|}$ and the angle-averaged quantity

$$\bar{T}_l \equiv \frac{1}{c_l} \int_{-1}^{1} dx\, P_l(x) T(q_0, q_0, x, E)(E - E_{\mathrm{pol}}(l)).$$

As demonstrated in Table 2, we approach the poles from both sides and the numbers closest to the poles agree very well with the corresponding residues calculated directly from the partial-wave-projected problem.

Table 2. Determination of $\bar{T}_l \equiv 1/c_l \int_{-1}^{1} dx\, P_l(x) T(q_0, q_0, x, E)(E - E_{\mathrm{pol}}(l))$ as function of E close to the $l = 1$ and $l = 0$ poles. The values for the constants are $c_0 = 2$ and $c_1 = \frac{2}{3}$. The entry p.w. indicates the value determined from the partial-wave-projected problem

E [MeV]	$\hat{T}_1(E)$ [MeV fm^2]	E [MeV]	$\hat{T}_0(E)$ [MeV fm^2]
−14.60	1.08424	−189.8	4.37911
−14.61	1.08513	−189.9	4.37847
−14.62	1.08597	−190.0	4.37772
−14.63	1.08588	−190.1	4.37722
−14.64	1.08778	−190.2	4.37693
−14.65	1.08857	−190.3	4.37608
p.w.	1.08684	p.w.	4.37685

The angular dependence of $T(q_0, q_0, x, E)$ with $q_0 = \sqrt{m|E|}$ for energies close to the two poles is displayed in Fig. 7. Both parts of the figure show that near and at the pole the T-matrix exhibits the characteristic behaviour of the Legendre function associated with the angular-momentum quantum number of the corresponding bound state. In Fig. 8 we show the angular dependence of $T(q_0, q_0, x, E)$ in the whole energy range

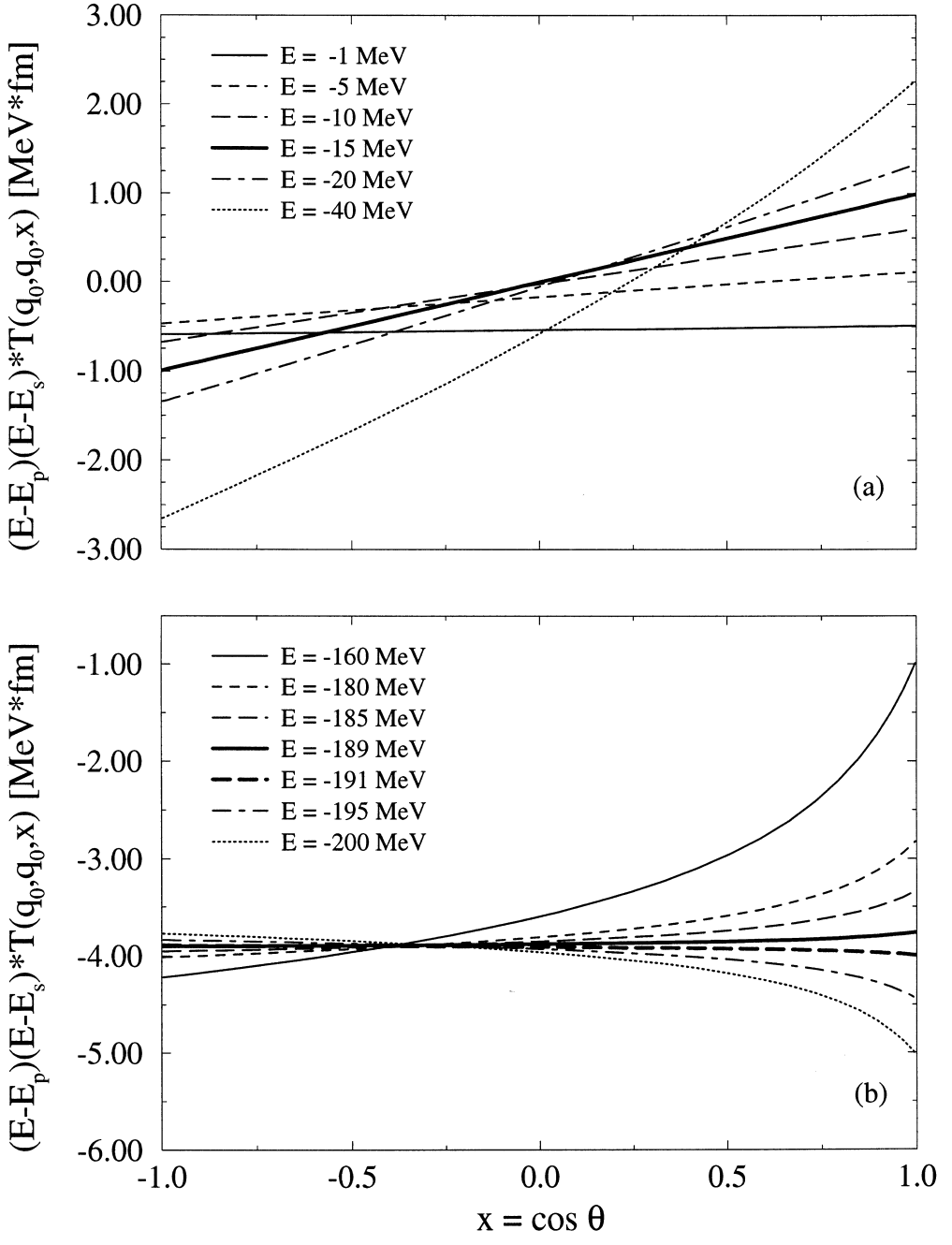

Fig. 7. Angular dependence of $(E - E_s)(E - E_p)T(q_0, q_0, x, E)$ for energies E around the p-wave pole (**a**) and the s-wave pole (**b**)

around and in between the bound-state poles. In order to include both poles we consider $(E - E_s)(E - E_p)T(q_0, q_0, x, E)$ in Figs. 7 and 8. Starting from very small values of $|E|$, the angular dependence is first of *s*-wave character, then turns to a *p*-wave shape at and near the *p*-wave pole, and then develops the forward peak known from corresponding positive energies. Note that due to the multiplicative factors, the peak turns upward in the two figures. When $|E|$ reaches the *s*-wave pole, T turns back to the pure *s*-wave behaviour and then finally flips back into a strong forward peak.

The fact that the angular dependence at negative energies is reminiscent of that at the corresponding positive energies, except for the characteristic behaviour near the poles, leads us to suspect that the real parts of T might be quite similar to each other at energies of equal magnitude. This turns out to be the case, as demonstrated in Fig. 9, where we display Re $T(q_0, q_0, x, E)$ for the potential $V^{(I)}$ for different values $|E|$. A similar result was found in ref. [10] for the partial-wave amplitudes of the off-shell *K*-matrix. It should be noted that the equality of Re $T(q_0, q_0, x, E)$ for positive and negative energies is not the trivial consequence of Re $T \approx V$, which does not hold. In order to demonstrate that V is significantly different from Re T, we also display V in Fig. 9. Comparing Re $T(q_0, q_0, x, E)$ at the different energies, we have to conclude that the rescattering terms, Re $T - V$, for the same absolute values of the energy become more and more similar to each other when the absolute value of the energy increases.

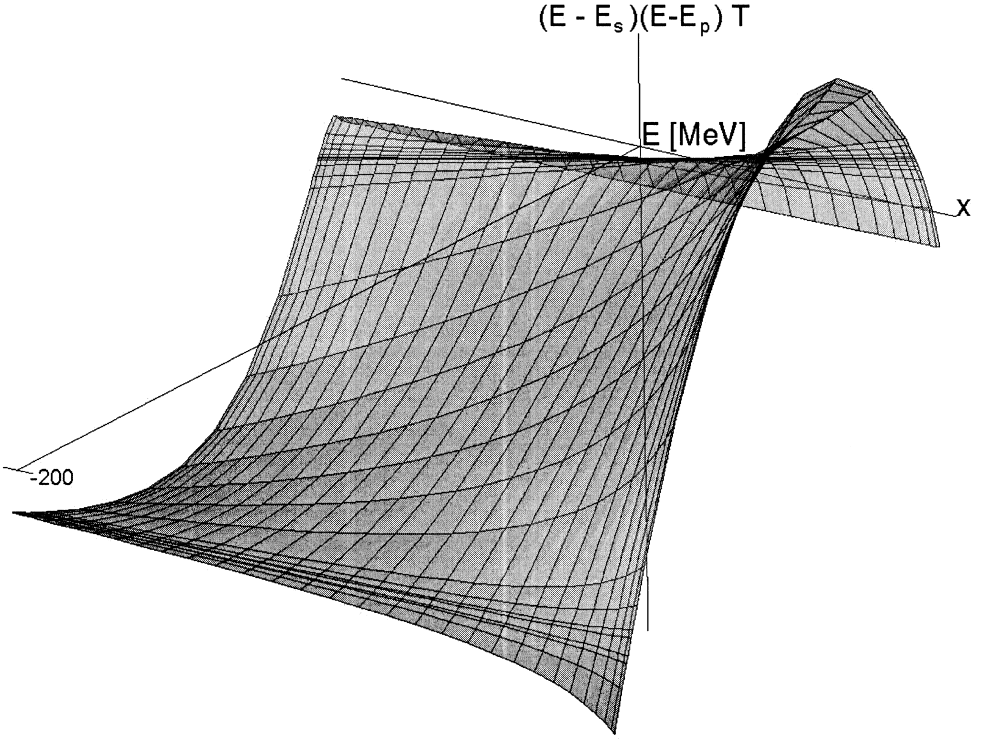

Fig. 8. Angular dependence of $(E - E_s)(E - E_p)T(q_0, q_0, x, E)$ as function of the energy from $E = -200\,\text{MeV}$ to $E = -1\,\text{MeV}$. Note the characteristic angular behaviour around the *p*- and *s*-wave poles as well as the strong forward peak between the two poles and below the *s*-wave pole

Finally, in Fig. 10 we display the real part of the fully off-shell T-matrix Re $T(q, q', x, E)$ as function of q and x for fixed energy $E = 200$ MeV and fixed momenta $q' = 250$ MeV/c and $q' = 1000$ MeV/c. As in Figs. 5 and 6 for positive energies, Re T is most strongly peaked at $q = q'$, what can be expected once the information of Figs. 5 and 6 is known.

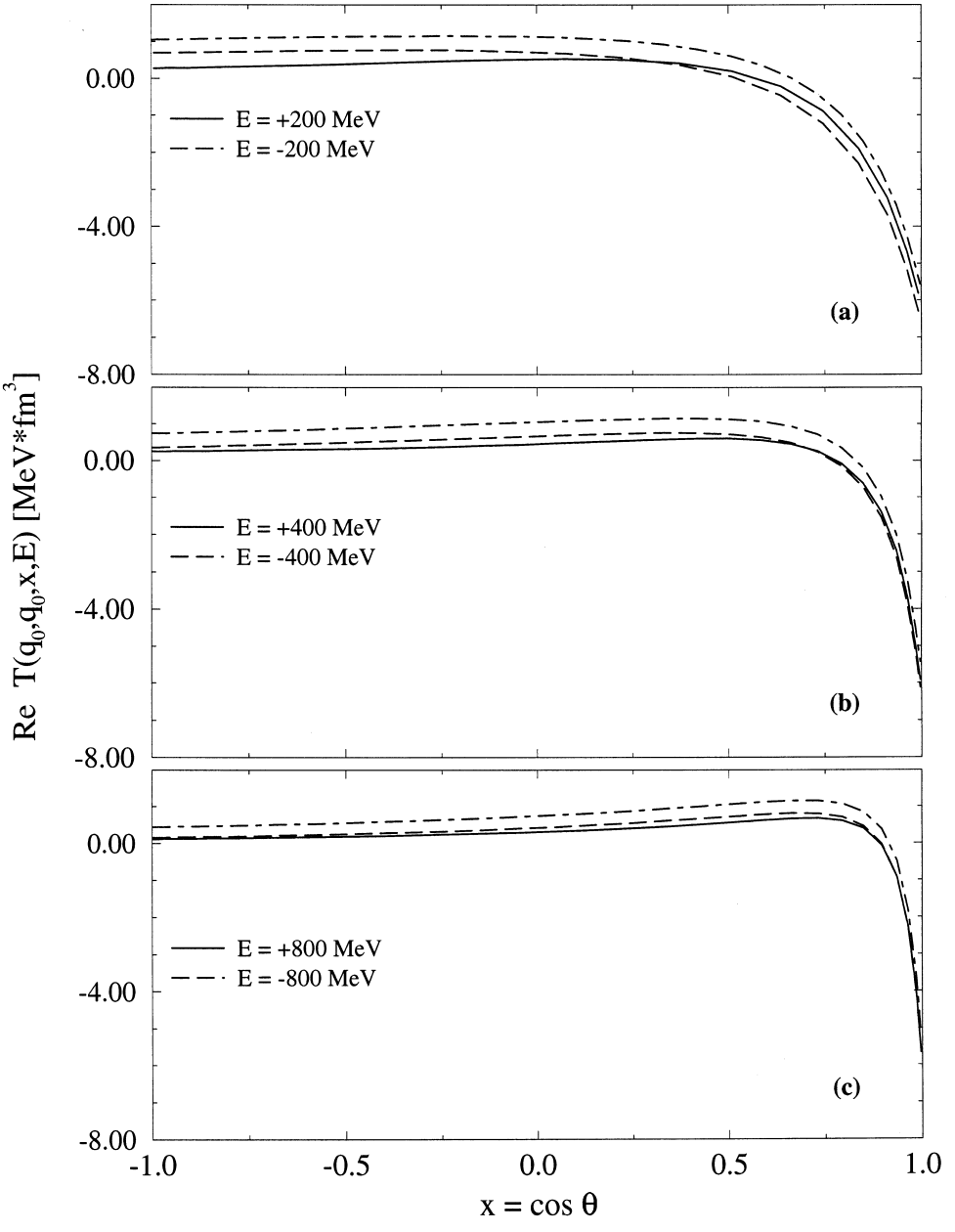

Fig. 9. Angular dependence of the real part of the on-shell T-matrix Re $T(q_0, q_0, x, E)$ for $|E| = 200$, 400, and 800 MeV. For comparison, the angular dependence of the driving term, V^{I}, is also shown as dash-dotted line

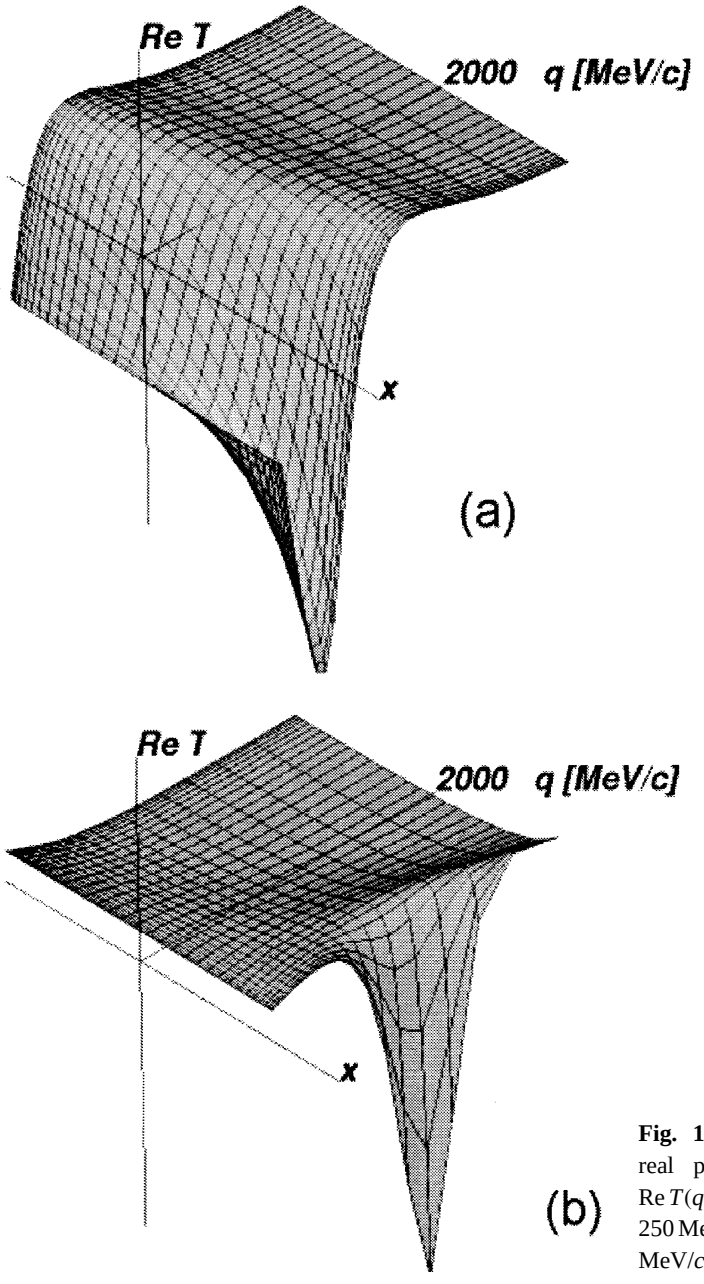

Fig. 10. Angular dependence of the real part of the off-shell *T*-matrix $\mathrm{Re}\,T(q, q', x, E = 200\,\mathrm{MeV})$ for $q' = 250\,\mathrm{MeV}/c$ (**a**) and for $q' = 1000\,\mathrm{MeV}/c$ (**b**)

4 The Off-Shell *T*-Matrix in the Second Energy Sheet

Two-body *T*-matrices might exhibit a resonant behaviour at positive energies or show a strong energy dependence near $E = 0$ due to a virtual state. This latter case is realized, for instance, in the *NN* system for the partial-wave state $^1S_0$. Our goal is to locate those resonances in the second energy sheet and investigate the characteristic angular dependence connected with the resonance or virtual state.

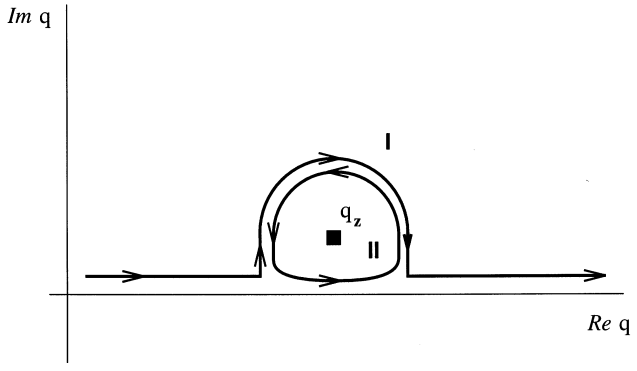

Fig. 11. Modified integration path in the complex q plane for the analytic continuation of the Lippmann-Schwinger equation into the second energy sheet as described in the text

The transition to the second energy sheet requires an analytic continuation of the Lippmann-Schwinger equation, Eq. (2.2), into the second energy sheet, which we briefly describe here [9]. For a complex energy z located in the upper half-plane, we modify the integration path as indicated in Fig. 11. The contribution along the closed path II gives a residue and we find

$$T(\mathbf{q}', \mathbf{q}, z) = V(\mathbf{q}', \mathbf{q}) - i\pi m q_z \int d\hat{q}''\ V(\mathbf{q}', \hat{\mathbf{q}}'' q_z) T(\hat{\mathbf{q}}'' q_z, \mathbf{q}, z) + \int_{\cap} d^3 q''\ V(\mathbf{q}', \mathbf{q}'') \frac{1}{z - \dfrac{q''^2}{m}} T(\mathbf{q}'', \mathbf{q}, z). \tag{4.1}$$

Here, $q_z = \sqrt{mz}$ is the magnitude of the complex momentum vector $\hat{\mathbf{q}}'' q_z$, and the symbol at the second integral indicates the deformed integration path I. Since we deformed the integration path such that it is located above the energy z, we are able to take z into the lower half of the complex plane without hitting a singularity in the propagator. Once the energy z is located in the lower half-plane, we can return with the integration path I to the real axis and have instead of Eq. (4.1)

$$T(\mathbf{q}', \mathbf{q}, z) = V(\mathbf{q}', \mathbf{q}) - i\pi m q_z \int d\hat{q}''\ V(\mathbf{q}', \hat{\mathbf{q}}'' q_z) T(\hat{\mathbf{q}}'' q_z, \mathbf{q}, z) + \int d^3 q''\ V(\mathbf{q}', \mathbf{q}'') \frac{1}{z - \dfrac{q''^2}{m}} T(\mathbf{q}'', \mathbf{q}, z). \tag{4.2}$$

This equation is valid on the second energy sheet, which is reached from the upper rim of the cut along the positive real-energy axis in the physical sheet. Due to the additional imaginary term, Eq. (4.2) has to be supplemented by another equation, which we obtain by choosing $\mathbf{q}' = \hat{\mathbf{q}} q_z$,

$$T(\hat{\mathbf{q}}' q_z, \mathbf{q}, z) = V(\hat{\mathbf{q}}'' q_z, \mathbf{q}) - i\pi m q_z \int d\hat{q}''\ V(\hat{\mathbf{q}}' q_z, \hat{\mathbf{q}}'' q_z) T(\hat{\mathbf{q}}'' q_z, \mathbf{q}, z) + \int d^3 q''\ V(\hat{\mathbf{q}}' q_z, \mathbf{q}'') \frac{1}{z - \dfrac{q''^2}{m}} T(\mathbf{q}'', \mathbf{q}, z). \tag{4.3}$$

Similar to the bound state, which induces a nontrivial solution for the homogeneous equation related to Eq. (2.1), the homogeneous set of equations related to Eqs. (4.2) and (4.3) has a nontrivial solution at discrete values of z. These discrete values either correspond to resonances with Re $z > 0$ and Im $z < 0$ or to virtual states with Re $z < 0$ and Im $z = 0$. The fact that this homogeneous set of equations has a nontrivial solution together with the compactness property of the integral kernel means that $T(z)$ has a pole at those energies z. We are interested not only in determining the positions of those poles but also in understanding the residues and their angular dependence.

As it is obvious from Eq. (4.3), the driving term singles out the first entry as complex number. In order to simplify the formal steps leading to a determination of the residue, it is convenient to supplement the set of equations given in Eqs. (4.2) and (4.3) by another set in which the driving term has a complex entry in the second argument. The two sets can then be combined using the following matrix notation

$$\begin{pmatrix} T(\mathbf{q}',\mathbf{q},z) & T(\mathbf{q}',\hat{\mathbf{q}}'q_z,z) \\ T(\hat{\mathbf{q}}'q_z,\mathbf{q},z) & T(\hat{\mathbf{q}}'q_z,\hat{\mathbf{q}}q_z,z) \end{pmatrix}$$

$$= \begin{pmatrix} V(\mathbf{q}',\mathbf{q}) & V(\mathbf{q}',\hat{\mathbf{q}}'q_z) \\ V(\hat{\mathbf{q}}'q_z,\mathbf{q}) & V(\hat{\mathbf{q}}'q_z,\hat{\mathbf{q}}q_z) \end{pmatrix} + \begin{pmatrix} \int d^3q''\ V(\mathbf{q}',\mathbf{q}'') & q_z^3 \int d\hat{q}''\ V(\mathbf{q}',\hat{\mathbf{q}}''q_z) \\ \int d^3q''\ V(\hat{\mathbf{q}}'q_z,\mathbf{q}'') & q_z^3 \int d\hat{q}''\ V(\hat{\mathbf{q}}'q_z,\hat{\mathbf{q}}''q_z) \end{pmatrix}$$

$$\times \begin{pmatrix} 1/[z-(q''^2/m)] & 0 \\ 0 & -i\pi(m/q_z^2) \end{pmatrix} \begin{pmatrix} T(\mathbf{q}'',\mathbf{q},z) & T(\mathbf{q}'',\hat{\mathbf{q}}q_z,z) \\ T(\hat{\mathbf{q}}''q_z,\mathbf{q},z) & T(\hat{\mathbf{q}}''q_z,\hat{\mathbf{q}}q_z,z) \end{pmatrix}. \tag{4.4}$$

Introducing the appropriate matrices, we write Eq. (4.4) as

$$\tilde{\mathbf{T}} = \tilde{\mathbf{V}} + \tilde{\mathbf{V}}\tilde{\mathbf{G}}\tilde{\mathbf{T}}. \tag{4.5}$$

We also need to study the corresponding homogeneous problem, which we want to write in the following form

$$\lambda(z)\tilde{\chi} = \tilde{\mathbf{V}}\tilde{\mathbf{G}}\tilde{\chi}. \tag{4.6}$$

In this form the eigenvalue is $\lambda(z)$ and the energy z is a parameter. Since $\tilde{\mathbf{V}}\tilde{\mathbf{G}}$ is a compact operator, there is a discrete set of eigenvalues, which accumulate at $\lambda(z) = 0$ [11]. The physical resonances occur at those values $z \equiv E_{\text{res}}$, for which $\lambda(E_{\text{res}}) = 1$. In the following we choose $z = E_{\text{res}}$. Then we have

$$\tilde{\chi} = \tilde{\mathbf{V}}\tilde{\mathbf{G}}\tilde{\chi}. \tag{4.7}$$

Since the kernel is nonsymmetric, we also have to consider the left-hand eigenvalue problem

$$\tilde{\boldsymbol{\Theta}}^T = \tilde{\boldsymbol{\Theta}}^T\tilde{\mathbf{V}}\tilde{\mathbf{G}}. \tag{4.8}$$

Defining

$$\tilde{\boldsymbol{\Phi}}^T \equiv \tilde{\boldsymbol{\Theta}}^T\tilde{\mathbf{V}} \tag{4.9}$$

we deduce

$$\tilde{\boldsymbol{\Phi}}^T = \tilde{\boldsymbol{\Phi}}^T\tilde{\mathbf{G}}\tilde{\mathbf{V}} \tag{4.10}$$

or

$$\tilde{\mathbf{\Phi}} = \tilde{\mathbf{V}}^T \tilde{\mathbf{G}} \tilde{\mathbf{\Phi}}. \tag{4.11}$$

Since $\tilde{\mathbf{V}}^T = \tilde{\mathbf{V}}$, we obtain $\tilde{\mathbf{\Phi}} = \tilde{\chi}$.

In the immediate neighborhood of $z = E_{\rm res}$ and as a consequence of

$$\tilde{\mathbf{T}}(z) = (1 - \tilde{\mathbf{V}}\tilde{\mathbf{G}})^{-1}\tilde{\mathbf{V}} \tag{4.12}$$

one has

$$\tilde{\mathbf{T}}(z) \xrightarrow{z \to E_{\rm res}} \tilde{\chi}(1 - \lambda(z))^{-1} \frac{1}{N} \tilde{\mathbf{\Theta}}^T \tilde{\mathbf{V}}, \tag{4.13}$$

where N is a normalization factor. In the neighborhood of $z = E_{\rm res}$ we can put

$$\lambda(z) \approx 1 + \lambda'(z)|_{z=E_{\rm res}} (z - E_{\rm res}) \tag{4.14}$$

and obtain

$$\tilde{\mathbf{T}}(z) \xrightarrow{z \to E_{\rm res}} \tilde{\chi} \frac{1}{z - E_{\rm res}} \frac{-1}{\lambda'(z)|_{z=E_{\rm res}}} \frac{1}{N} \tilde{\chi}^T. \tag{4.15}$$

For the case of a bound-state pole it is easy to prove that

$$\frac{-1}{\lambda'(z)|_{z=E_{\rm res}}} \frac{1}{N} = 1$$

for a normalized bound state $|\phi_b\rangle$ and $|\chi\rangle = V|\phi_b\rangle$. If we consider the right-hand side of Eq. (4.15) as function of an auxiliary strength factor to the potential, we can adopt the normalization of the bound state and define

$$\tilde{\mathbf{T}}(z) \xrightarrow{z \to E_{\rm res}} \tilde{\chi} \frac{1}{z - E_{\rm res}} \tilde{\chi}^T. \tag{4.16}$$

The final remark concerns the scalar nature of $\tilde{\mathbf{T}}(\mathbf{q}', \mathbf{q}, z)$. Since a resonant state has a unique angular momentum l, the function $\chi(\mathbf{q})$ will have the form

$$\chi(\mathbf{q}) = \chi_l(q) Y_{lm}(\hat{\mathbf{q}}), \tag{4.17}$$

and we have to conclude that

$$\tilde{\mathbf{T}}(\mathbf{q}', \mathbf{q}, z) \xrightarrow{z \to E_{\rm res}} \frac{2l+1}{4\pi} \chi_l(q') \frac{1}{z - E_{\rm res}} \chi_l(q) P_l(\hat{\mathbf{q}}' \cdot \hat{\mathbf{q}}). \tag{4.18}$$

If Re $E_p > 0$ and if Im $E_p < 0$ is sufficiently small, the T-matrix will feel the nearby pole also for real, positive energies z, and a resonance will occur in the differential cross section. In the case of a virtual state, like for $^1S_0$ in NN scattering, the pole is located at Re $E_p < 0$ and Im $E_p = 0$. For sufficiently small values of $|\mathrm{Re}\, E_p|$ the T-matrix will be strongly enhanced near and at $z = 0$.

For our numerical realization we rewrite Eqs. (4.2) and (4.3) analogously to Eq. (2.8) as

$$\begin{aligned} T(q', q, x') = & \frac{1}{2\pi} v(q', q, x, 1) \\ & + \int_0^\infty dq''\ q''^2 \int_{-1}^{1} dx''\ v(q', q'', x', x'') \frac{1}{z - \dfrac{q''^2}{m}} T(q'', q, x'') \end{aligned}$$

$$-i\pi m q_z \int_{-1}^{1} dx''\ v(q', q_z, x', x'') T(q_z, q, x'') \tag{4.19}$$

and

$$\begin{aligned} T(q_z, q, x') = & \frac{1}{2\pi} v(q_z, q, x, 1) \\ & + \int_0^\infty dq''\ q''^2 \int_{-1}^{1} dx''\ v(q_z, q'', x', x'') \frac{1}{z - \dfrac{q''^2}{m}} T(q'', q, x'') \\ & - i\pi m q_z \int_{-1}^{1} dx''\ v(q_z, q_z, x', x'') T(q_z, q, x''). \end{aligned} \tag{4.20}$$

Here $z \equiv E = |E| e^{i\phi}$ with $\phi < 0$ and $q_z = \sqrt{mE} = \sqrt{m|E|} e^{i\phi/2}$. The nontrivial solution to the homogeneous system of Eq. (4.7) has a fixed angular momentum. When employing Eq. (4.17), we obtain

$$\chi_l(q) = \int_0^\infty dq'\ q'^2 v_l(q, q') \frac{1}{z - \dfrac{q'^2}{m}} \chi_l(q') - i\pi m q_z v_l(q, q_z) \chi_l(q_z) \tag{4.21}$$

and

$$\chi_l(q_z) = \int_0^\infty dq'\ q'^2 v_l(q_z, q') \frac{1}{z - \dfrac{q'^2}{m}} \chi_l(q') - i\pi m q_z v_l(q_z, q_z) \chi_l(q_z). \tag{4.22}$$

We used the above equations (4.21) and (4.22) to determine the location of the resonances in the second energy sheet. For *s*-waves they are usually called virtual states and are located on the negative-energy axis. For partial waves with $l = 1$ or higher, the energy eigenvalues have a positive real part and a negative imaginary part. For varying potential strength, they move along trajectories in the complex energy plane. In the following, we numerically study two different cases, namely a *s*-wave virtual state

Table 3. Pole trajectories in the complex energy plane as function of the strength parameter V_A for the potentials $V^{(\mathrm{III})}$ (*p*-wave pole trajectory) and $V^{(\mathrm{IV})}$ (*s*-wave virtual-state trajectory)

V_A ($V^{(\mathrm{III})}$)	$E_{\mathrm{res}}(l=1)$ [MeV]	V_A ($V^{(\mathrm{IV})}$)	$E_{\mathrm{res}}(l=0)$ [MeV]
5.4	$0.9267 - i\,0.1821$	2.6047	−0.06663
5.3	$2.1972 - i\,0.7101$	2.6	−0.07380
5.2	$3.3254 - i\,1.4134$	2.5	−0.31004
5.1	$4.3177 - i\,2.2386$	2.4	−0.69870
5.0	$5.1801 - i\,3.1552$	2.3	−1.22970
4.9	$5.9178 - i\,4.1413$	2.2	−1.89300
4.8	$6.5358 - i\,5.1806$	2.1	−2.67878
4.7	$7.0388 - i\,6.2597$	2.0	−3.57733

supported by potential model $V^{(\mathrm{IV})}$ of Table 1 and a p-wave resonance of potential model $V^{(\mathrm{III})}$ of Table 1. The corresponding trajectories are listed in Table 3.

For the case of the s-wave virtual state we started from potential model $V^{(\mathrm{IV})}$ of Table 1. The s-wave phase shift of this potential has an effective-range expansion with a scattering length $a_s = -23.5818$ fm and an effective range $r_s = 2.8789$ fm. Using these values, the pole position for the S-matrix can be estimated via the effective-range expansion as

$$q_v^a = i\left[\frac{1}{r_s} - \sqrt{\frac{2}{r_s|a_s|} + \frac{1}{r_s^2}}\right], \tag{4.23}$$

which leads in our specific case to a position of the virtual state

$$E_{q_v}^a = -\frac{(q_v^a)^2}{m} = -0.06738\,\mathrm{MeV},$$

where we used $m = 938.9$ MeV. This number is very close to the exactly calculated value given as $E_p(l=0) = -0.06663$ MeV, quoted in Table 3. In the same table we quantify the s-wave trajectory as a function of the strength parameter V_A of potential $V^{(\mathrm{IV})}$.

For obtaining a p-wave resonance state, we start from potential $V^{(\mathrm{II})}$ of Table 1, which supports a p-wave bound state, and decrease the attraction by decreasing the strength parameter V_A until the bound state turns into a resonance state. Selected values for the so obtained trajectory for the p-wave resonance are listed in Table 3. Of course, this model does not correspond to the reality of an NN force, even for the lowest value of $V_A = 4.7$ given in Table 3, the binding energy of the s-wave bound state is still $E_s = -52.52$ MeV. Nevertheless, this example illustrates in a simple manner, what can be expected for other cases like an effective nucleon-nucleus interaction, which supports low-energy resonances for certain angular-momentum states. Qualitatively the same picture would emerge.

We would like to mention that we solved the homogeneous set of Eqs. (4.21) and (4.22) by the very efficient power method [7, 9]. Regarding the notation of Eq. (4.7), one has to determine the eigenvalue $\lambda(z)$ and vary the energy such that $\lambda(z) = 1$. For the potentials used here, the largest eigenvalue in magnitude was always an unphysical one with a negative real part generated by the repulsive short-range piece of the force. Once the largest eigenvalue is determined, we introduce a new integral kernel, consisting of the old one minus that specific eigenvalue. The new kernel defined in this way has then the physical eigenvalue as the largest one in magnitude.

Next we investigate the solution of the T-matrix in the second energy sheet as given by Eqs. (4.19) and (4.20). We are interested in verifying the location of the pole as well as the angular dependence of the residue at the pole as given in Eq. (4.18). We illustrate our findings for the potential $V^{(\mathrm{III})}$ of Table 1, which has a p-wave resonant state at $E_{\mathrm{res}}(l=1) = (4.3177 - i2.2386)$ MeV, and for the potential $V^{(\mathrm{IV})}$ of Table 1, which has a virtual s-wave state at $E_{\mathrm{res}}(l=0) = -0.06663$ MeV. For the p-wave resonance we show in Figs. 12 and 13 the angular dependence of $\mathrm{Re}[(E - E_{\mathrm{res}}(l=1))T(q_E, q_0, x, E)]$ as function of the complex energy E located along two straight lines going through the pole position. In Fig. 12 we start on the real axis at $E = 4.3$ MeV and successively increase the imaginary part of E. For

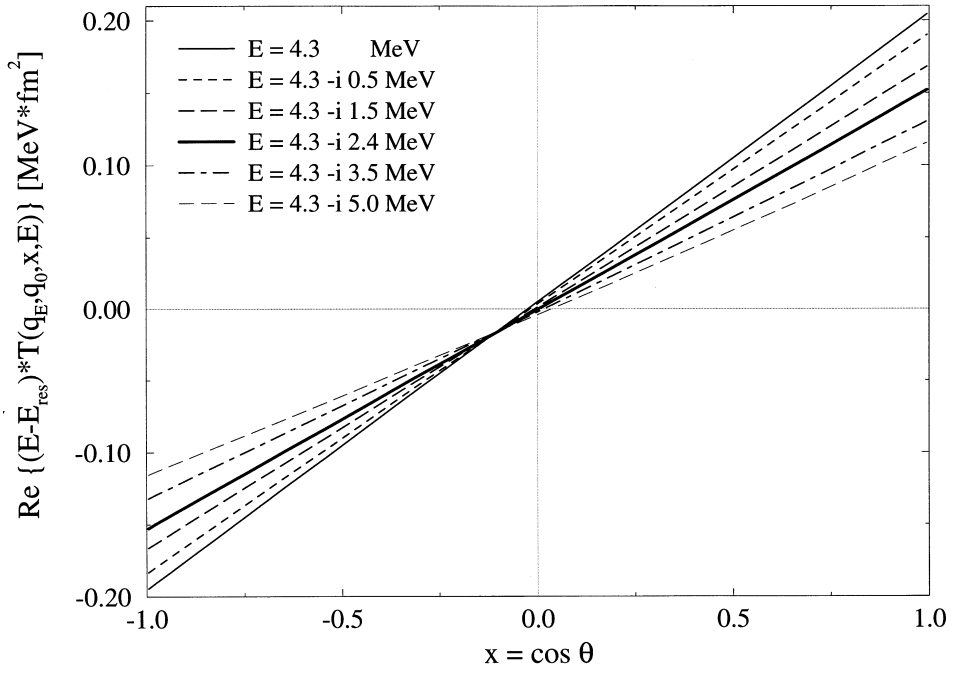

Fig. 12. Angular dependence of the real part of $(E - E_{\rm res})T(q_E, q_0, x, E)$ as function of the complex energy E around the p-wave resonance of potential model $V^{(\rm III)}$. The off-shell momentum q_0 is fixed at 100 MeV/c

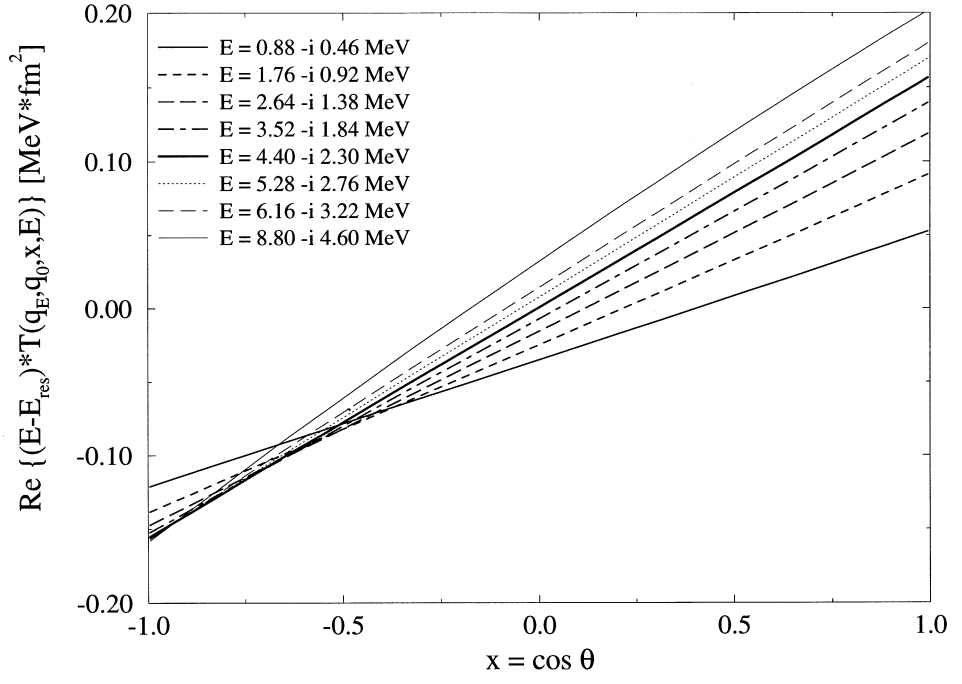

Fig. 13. Same as Fig. 12, but for a different path of the complex energy E

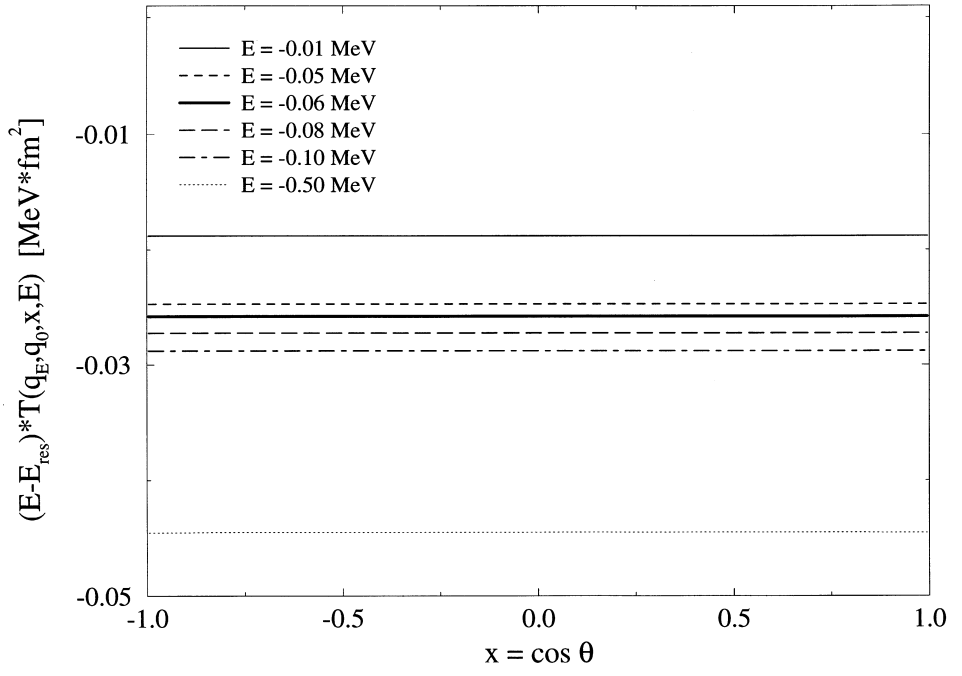

Fig. 14. Angular dependence of $(E - E_{\rm res})T(q_E, q_0, x, E)$ as function of the negative energy E in the second energy sheet around the s-wave virtual state of potential model $V^{(\rm IV)}$. The off-shell momentum q_0 is fixed at 100 MeV/c

$E = (4.3 - i2.4)$ MeV we clearly see an angular dependence characteristic of a p-wave residue. Since the width of the resonance is relatively small, the p-wave behaviour is present along the whole vertical energy line including the point on the real axis. For our second choice of energy line (Fig. 13), a declined line starting from zero energy, begins with a behaviour being a mixture of s- and p-wave, but still relatively flat. Approaching the resonance, the shape becomes predominantly the one of a $P_1(x)$ given by the p-wave residue.

A corresponding study based on the potential model $V^{(\rm IV)}$ is shown in Fig. 14 for the negative real axis in the second sheet, where the neighborhood of the virtual-pole position is considered. In the vicinity of the virtual state, the residue exhibits perfect s-wave characteristics.

Finally, we would like to demonstrate the structure of the T-matrix as given in Eq. (4.18) in a numerical example. First, we verify numerically that $\lim_{z\to E_{\rm res}}(z - E_{\rm res})T(q', q, x, z)$ behaves like $P_1(z)$. Then we determine $\chi_1(q)$ by comparing the numerically calculated quantity $(z - E_{\rm res})T(q', q, x, z)$ to the form given in Eq. (4.18). Instead of dividing by $P_1(x)$ we use

$$\bar{\chi}_1(q) = \lim_{z\to E_{\rm res}} \sqrt{2\pi \int_{-1}^{1} dx\; P_1(x)(z - E_{\rm res})T(q, q, x, z)}. \tag{4.24}$$

The values of $\bar{\chi}_1(q)$ for z approaching $E_{\rm res}$ are shown for a few arbitrarily selected momentum points q in Table 4. They stabilize for z approaching the pole position

Table 4. Determination of $\bar{\chi}_1(q)$ in the vicinity of the *p*-wave resonance of potential model $V^{(\mathrm{III})}$ as function of the complex energy E

E [MeV]	$\bar{\chi}_1$ ($q = 94.89\,\mathrm{MeV}/c$)	$\bar{\chi}_1$ ($q = 292.73\,\mathrm{MeV}/c$)	$\bar{\chi}_1$ ($q = 527.50\,\mathrm{MeV}/c$)	$\bar{\chi}_1$ ($q = 758.09\mathrm{MeV}/c$)
$4.32 - i\,2.0$	$1.105 - i\,0.400$	$1.856 - i\,0.729$	$1.149 - i\,0.473$	$0.491 - i\,0.212$
$4.32 - i\,2.10$	$1.103 - i\,0.400$	$1.851 - i\,0.729$	$1.144 - i\,0.471$	$0.488 - i\,0.207$
$4.32 - i\,2.20$	$1.101 - i\,0.400$	$1.846 - i\,0.729$	$1.139 - i\,0.468$	$0.484 - i\,0.202$
$4.32 - i\,2.23$	$1.101 - i\,0.400$	$1.844 - i\,0.729$	$1.138 - i\,0.467$	$0.483 - i\,0.201$
$4.32 - i\,2.4$	$1.098 - i\,0.400$	$1.835 - i\,0.729$	$1.129 - i\,0.461$	$0.477 - i\,0.192$
$4.32 - i\,2.5$	$1.096 - i\,0.400$	$1.830 - i\,0.729$	$1.124 - i\,0.459$	$0.473 - i\,0.187$
p.w.	$1.102 - i\,0.400$	$1.844 - i\,0.729$	$1.138 - i\,0.468$	$0.482 - i\,0.200$

Table 5. Comparison of $\bar{T} = 2\pi \int_{-1}^{1} dx\, P_1(x)(E - E_{\mathrm{res}})T(q, q', x, E)$ with $\bar{\chi}_1(q)\bar{\chi}_1(q')$ for a fixed value q' and different values of q at the *p*-wave resonance of potential model $V^{(\mathrm{III})}$. The energy E for calculating $\bar{T}$ was fixed at $E = (4.32 - i2.23)\,\mathrm{MeV}$

q [MeV/c]	q' [MeV/c]	$\bar{T}$ [MeV fm^2]	$\bar{\chi}_1(q)\bar{\chi}_1(q')$ [MeV fm^2]
292.73	94.89	$1.7398 - i\,1.5395$	$1.7397 - i\,1.5398$
527.50	94.89	$1.0668 - i\,0.9683$	$1.0667 - i\,0.9689$
758.09	94.89	$0.4522 - i\,0.4134$	$0.4521 - i\,0.4140$

$E_{\mathrm{res}} = (4.318 - i2.239)\,\mathrm{MeV}$. The last row in Table 4 shows the values obtained from the solution of the homogeneous set of Eqs. (4.21) and (4.22). They have been normalized at one q point to the $\chi_1(q)$ extracted from $T(q, q, x, z \to E_{\mathrm{res}})$. The agreement is perfect.

Finally, we directly verified the separable structure of $T(q', q, x, z \to E_{\mathrm{res}})$ as given in Eq. (4.18) by evaluating

$$\tilde{T} = 2\pi \int_{-1}^{1} dx\, P_1(x)(E - E_{\mathrm{res}})T(q', q, x, E)$$

very close to $E = E_{\mathrm{res}}$ for different $q' \neq q$ and comparing them to the values obtained via Table 4. The agreement is again perfect and the values for a selected set of momentum points q' and q are given in Table 5.

5 Summary

Two-nucleon scattering at intermediate energies of a few hundred MeV requires quite a few angular-momentum states in order to achieve convergence of, e.g., scattering observables. This is even more true for the scattering of three or more nucleons on each other. An alternative approach to the conventional one, which is based on angular-momentum decomposition, is to work directly with momentum vectors, specifically with the magnitudes of the momenta and the angles between them. We

formulated and numerically illustrated this alternative approach for the case of two-body scattering, bound states, and resonances. The angular dependence of the two-body T-matrix is directly determined from the Lippmann-Schwinger equation, which now is a two-dimensional integral equation in contrast to the one-dimensional one for a fixed angular momentum in a partial-wave formulation. This two-dimensional integral equation is quite easily tractable numerically. We determined the angular dependence of the on-shell, half-off-shell and fully off-shell T-matrices as functions of the scattering energy and different choices of momenta. As two-body force we concentrated on a superposition of an attractive and repulsive Yukawa interaction, which is typical for nuclear physics. We neglected spin degrees of freedom in all our studies.

The on-shell T-matrix develops a strong forward peak as the energy increases, which is more and more difficult to build up in a calculation based on angular-momentum decomposition, but relatively simple accessible in our approach using momentum vectors. The angular dependence of the half-off-shell T-matrix is strong only around the on-shell momentum and rather mild otherwise. For a fully off-shell T-matrix $T(q, q', x, E)$ a strong angular dependence occurs for momenta $q = q'$, which do not necessarily have to coincide with the on-shell momentum. At negative energies the T-matrix has poles located at the bound-state energies, if those exist. As example we investigated s- and p-wave bound states. The numerically determined T-matrix turned out to be very well under control even quite close to the bound-state poles, where the homogeneous version of the Lippmann-Schwinger equation has a nontrivial solution. We determined the angular dependence of the T-matrix at the two poles, at energies between them, and at energies way below the deepest bound state. Directly at the poles the angular behaviour displays the characteristics of the Legendre polynomial of the same angular momentum l as the bound state. Between the poles as well as for energies below the last bound state the T-matrix exhibits the same forward peaking as visible at positive energies. This latter result is interesting by itself. The angular dependence at positive and negative energies is very similar. More quantitatively, we found that the real parts of the T-matrix are extremely close to each other at positive and negative energies of equal magnitude long before this statement becomes trivial due to the validity of the zeroth order Born approximation $T = V$.

Finally we studied the analytical continuation of the Lippmann-Schwinger equation into the second energy sheet, which is reached through the cut along the positive real axis of the physical sheet. In the lower half-plane possible resonance poles of the T-matrix are located, which are, of course, of interest only if they are close to the real axis. As example we studied a p-wave resonance and mapped out its pole trajectory by varying the potential strength. At the pole, the T-matrix assumes a separable form, which we verified numerically. We also found the characteristic angular dependence of the T-matrix close to the resonance, which corresponds to the Legendre polynomial of degree l of the angular-momentum state of the resonance. For negative energies in the second sheet we investigated the pole trajectory of a virtual s-wave state, which is of interest in the NN system for the quantum number $^1S_0$.

Summarizing we can state that the two-dimensional Lippmann-Schwinger equation can be handled quite easily in a manner very reliable numerically. In this approach one determines directly the angular dependence of the T-matrix for arbitrary momenta and energies. Once supplemented by spin degrees of freedom this approach will be of

interest in the *NN* system. In addition, this approach will be generalizable to systems with three particles, like three nucleons or two nucleons and a meson. In the case of three nucleons, Faddeev calculations at an energy of, e.g., 150 MeV and higher are getting quite tedious because of the very many orbital-angular-momentum states involved [8] and a direct, three-dimensional approach appears to be preferable. First steps in this direction are under way.

Acknowledgments. This work was performed in part under the auspices of the U.S. Department of Energy under contract No. DE-FG02-93ER40756 with Ohio University and the NATO Collaborative Research Grant 960892. We thank the Ohio Supercomputer Center (OSC) for the use of their facilities under Grant No. PHS206. The authors would like to thank S. P. Weppner and X. D. Zhang for their help in preparing some of the figures.

References

1. Holz, J., Glöckle, W.: Phys. Rev. **C37**, 1386 (1988); Holz, J., Glöckle, W.: J. Comp. Phys. **76**, 131 (1988)
2. Rice, R. A., Kim, Y. E.: Few-Body Systems **14**, 127 (1993)
3. Hiltrop, J.: Diploma Thesis, Bochum, 1989 (unpublished); Posukidis, I.: Diploma Thesis, Bochum, 1993 (unpublished)
4. Hüber, D., Glöckle, W., Bömelburg, A.: Phys. Rev. **C42**, 2342 (1990)
5. Machleidt, R., Holinde, K., Elster, Ch.: Phys. Rep. **149**, 1 (1987)
6. Redish, E. F., Stricker-Bauer, K.: Phys. Rev. **C36**, 513 (1987)
7. Malfliet, R. A., Tjon, J. A.: Nucl. Phys. **A127**, 161 (1969)
8. Glöckle, W., Witała, H., Hüber, D., Kamada, H., Golak, J.: Phys. Rep. **274**, 107 (1996)
9. Glöckle, W.: The Quantum Mechanical Few-Body Problem. Berlin Heidelberg New York: Springer 1983
10. Delfino, A., Redish, E. F.: In: Proceedings of the 13th International Conference on Few-Body Problems in Physics, Adelaide, 1992, Book of Contributions (Afnan, I. R., Cahill, R. T., eds.), p. 148. Adelaide: Institute for Atomic Studies 1992
11. Weinberg, S.: Phys. Rev. **B133**, 232 (1964)

Received May 29, 1997; revised October 17, 1997; accepted for publication December 28, 1997